

Niğde Ömer Halisdemir Üniversitesi Mühendislik Bilimleri Dergisi Niğde Ömer Halisdemir University Journal of Engineering Sciences

Araştırma makalesi / Research article

www.dergipark.org.tr/tr/pub/ngumuh / www.dergipark.org.tr/en/pub/ngumuh



A numerical study on the lateral torsional buckling behaviour of aluminium/CFRP hybrid I-beam

Alüminyum/KETP hibrit I-kirişin yanal burulma burkulma davranışı üzerine nümerik bir çalışma

Hamza Tas^{1,*}

¹Manisa Celal Bayar University, Department of Mechanical Engineering, 45400, Manisa, Türkiye

Abstract

This work intends to numerically investigate the impacts of bonding carbon fibre reinforced polymer (CFRP) laminates to either the web or the flange of 6061-T6 aluminium alloy I-beam on the lateral torsional buckling (LTB) characteristic. The effect of laminate thickness, fibre orientation angle, laminate length, and laminate location was examined. In all hybrid I-beams, web and flange thicknesses were kept equal to those of aluminium (Reference) I-beam. Finite element (FE) models of aluminium and aluminium/CFRP hybrid I-beams were developed using Abaqus/Standard. Model verification was carried out by comparison of the numerical findings with experimental results available in the existing literature. A strong concordance was observed between the experimental and numerical findings, with a relative error of 3.3% at the critical LTB bending moment (M_{cr}). Attaching a 3 mm-thick CFRP laminate, aligned at 0° fibre orientation, to the flange of an I-beam increases the M_{cr} by 47.5% compared to the aluminium I-beam.

Keywords: Lateral torsional buckling, Finite element analysis, Hybrid I-beam, Aluminium, Carbon fibre reinforced polymer

1 Introduction

Lateral-torsional buckling (LTB) is a prevalent instability event observed in slender structural members subjected to bending. The cross-section undergoes both lateral displacement and twisting simultaneously along the entire length of the member [1].

Aluminium structural members are favoured in construction applications such as roof structures, transmission towers, curtain walls, and portable bridges because they are lightweight, resist corrosion well, require minimal maintenance, and have a long service life [2–4]. Numerous works have been conducted to examine the buckling characteristics of the aluminium structural members. Wang et al. [5] examined the LTB characteristics of I-beams made of Al6063-T5 and Al6061-T6, representing alloys with strong and weak hardening characteristics, respectively. Flange widths and unbraced length of the beams were designated as the geometric parameters for evaluating the LTB characteristic of the beams. In the case

Öz

Bu çalışma, karbon elyaf takviyeli polimer (KETP) laminatların 6061-T6 alüminyum alaşımlı I-kirişin gövdesine veya flanşına yapıştırılmasının yanal burulma burkulması (YBB) davranışına etkilerini nümerik olarak incelemeyi amaçlamaktadır. Laminat kalınlığı, fiber açısı, laminat uzunluğu ve laminat konumunun etkisi incelenmiştir. Tüm hibrit I-kirişlerde, gövde ve flanş kalınlıkları alüminyum (Referans) I-kiriş ile aynı tutulmuştur. Alüminyum ve alüminyum/CFRP hibrit kirislerin sonlu eleman (SE) modelleri Abagus/Standard kullanılarak oluşturulmuştur. Model doğrulaması, sayısal sonuçların mevcut literatürdeki deneysel sonuçlarla karşılaştırılmasıyla yapılmıştır. Kritik YBB eğilme momentinde (M_{kr}) %3.3 göreli hata ile sayısal ve deneysel sonuçlar arasında güçlü bir uyum gözlenmiştir. 0° fiber açısına sahip 3 mm kalınlığında KETP laminatın I-kirişin flanşına yapıştırılması, M_{kr} değerini alüminyum I-kirişe kıyasla %47.5 artırmaktadır.

Anahtar kelimeler: Yanal burulma burkulması, Sonlu elemanlar analizi, Hibrit I-kiriş, Alüminyum, Karbon elyaf takviyeli polimer

of long-span beams, the compression flanges began to deform laterally at relatively low loads, and this deformation gradually increased as the load approached its maximum value. In contrast, the short-span beams exhibited minimal lateral deformation up to the peak load, beyond which they experienced sudden failure. Guo et al. [6] examined the flexural-torsional buckling (FTB) characteristics of the 6061-T6 aluminium alloy T-beam and I-beam. Faella et al. [7] investigated the effect of the width-to-thickness (b/t) ratios on local buckling resistance of aluminium alloy hollow (rectangular and square) under compression. Based on the test results, an empirical formula was created to predict the average strain at ultimate resistance. Zhang et al. [8] performed a comprehensive experimental investigation on the FTB characteristics of Al6061-T6 unequal-leg angle columns under axial compression. The work examined the influences of aspect and width/thickness ratios on FTB responses. The results revealed that these geometric parameters had a crucial

^{*} Sorumlu yazar / Corresponding author, e-posta / e-mail: hamza.tas36@gmail.com (H. Taş) Geliş / Received: 29.06.2025 Kabul / Accepted: 30.07.2025 Yayımlanma / Published: 15.10.2025 doi: 10.28948/ngumuh.1729855

influence on the instability characteristics of the angle columns. Wang et al. [9] investigated the buckling characteristics of 7A04 HS aluminium alloy angle columns subjected to axial compression. Utilizing the finite element (FE) model, the influence of the angle legs' width-tothickness ratio, the strength of the material, and initial geometric imperfections on the load-bearing capability of angle columns were examined. The findings indicated that as the slenderness ratio increased, the influence of the width-tothickness ratio diminished and became negligible. The nominal yield stress has a negligible impact on the buckling response of thin-walled columns characterized by large slenderness and high width-to-thickness ratios. Xu et al. [10] examined the buckling strength of the aluminium alloy angle struts under axial compression loading, with lateral bracing on one leg. The buckling behaviour was found to be highly sensitive to the ratio between the flexural buckling load about the rectangular axis and the torsional buckling load.

Thin-walled pultruded composite beams are being also increasingly utilized in the construction sector, particularly in environments with high corrosion or in applications that demand rapid assembly and lightweight structural components [11]. Several studies have been conducted on the buckling behaviour of composite beams. Correia et al. [12] studied the buckling and post-buckling characteristics of the glass fibre reinforced polymer (GFRP) pultruded Ibeams. The experimental results from both simply supported cantilever beams clearly demonstrated failure mechanisms induced by the onset of local buckling and LTB. The critical LTB load of a pultruded E-glass reinforced polymer I-beam was determined experimentally and compared with the theoretical predictions by Mottram [13]. Davalos et al. [14] investigated the lateral-distortional and flexural-torsional buckling behaviour of FRP wide-flange beams through combined experimental and analytical methods. New models were created and verified with experimental findings. Results showed a good agreement between analytical and experimental results. Turvey [15] investigated lateral buckling characteristics of pultruded GFRP I-section cantilever beams with spans from 0.5 to 1.5 m under various point load positions. Moreover, experimental results were compared with buckling loads predicted by analytical and FE methods. It was found that predicted buckling loads were usually less than experimental loads. Qiao [16] focused on the FTB characteristics of pultruded FRP composite cantilever I-beams through analytical and experimental methods. They provided a simplified equation for predicting the flexural-torsional buckling load of FRP wide-flange beams. Lee et al. [17] examined the impacts of fibre orientation, load type, load location, and load type on the critical LTB loads of laminated composite I-beams. As the fibre orientation was rotated away from the principal axis, the lateral buckling load increased, reaching a maximum at a fibre angle of 45°, and then declined to its lowest value at a fibre angle of 90°. Furthermore, an increase in span length resulted in a decrease in the lateral buckling load. Kahya [18] developed a multilayer beam FE by employing the first-order shear deformation theory to compute vibration and buckling of laminated composite and sandwich beams, assuming no slip or delamination between layers. The element accurately predicted buckling loads for unidirectional, cross-ply, and sandwich beams. Barbero and Raftoyiannis [19] developed analytical models to predict local buckling in FRP thinwalled members exposed to shear and axial stresses, which effectively characterize the buckling behaviour of FRP beams

In recent years, strengthening structural members through the bonding of FRP plates has emerged as a viable and effective application [20]. Several studies have investigated the use of FRP plates for strengthening applications. Pham [21] investigated the elastic LTB characteristic of steel beams retrofitted with GFRP plates of which symmetrically balanced. A novel analytical theory using the total stationary buckling energy principle was created. A parametric study was performed to determine the impacts of laminate thickness, lamina properties, fibre orientation, adhesive shear modulus, and adhesive layer thickness on the buckling moment. According to the findings, GFRP laminates with ±45° fibre orientations significantly improved buckling resistance. Moreover, orthotropic GFRP laminate-retrofitted steel beams showed lower buckling resistance compared to those with isotropic laminates. In another study of Pham [22], three strengthening methods ((i) web stiffener, (ii) attaching GFRP plates to the flanges, and (iii) combination of (I) and (ii)) for wide flange steel beams were proposed. According to the findings, bonding the GFRP plates offered the highest improvement in moment capacity, while the web stiffener alone had limited effectiveness. Pham et al. [20] also reported that glueing GFRP laminates to the compression flange of steel beams was the most effective method for enhancing the LTB capacity, while application to the tension flange yielded only a moderate improvement. The buckling behaviour of steel Ibeams strengthened with carbon FRP (CFRP) laminates at various pre-stress levels was investigated experimentally and numerically by Ghafoori and Motavalli [23]. According to the results, elevating the pre-stress in CFRP laminates did not necessarily improve the instability load of slender steel beams. Harries et al. [24] applied FRP strips (ultra-high modulus GFRP strips or high-strength CFRP strips) to the steel WT stem. The samples retrofitted with GFRP strips demonstrated an increase in axial capacity ranging from 6% to 9%, whereas those strengthened with CFRP strips showed a small reduction in axial capacity relative to the unretrofitted control specimens. Accord and Earls [25] performed a FE-based work of I-beam wherein GFRP strips were glued to the I-beam's flange. The effects of the location of the GFRP strip across the flange width and the length of the GFRP strip were investigated. Shifting the GFRP strips toward the flange outstands led to a significant improvement in ultimate moment capacity. Reducing the GFRP strip length from 3.81 m to 1.905 m had a negligible impact on the ultimate moment capacity. However, a further drop in GFRP strip length to 0.762 m resulted in a noticeable decrease in the ultimate moment capacity. Damatty et al. [26] performed both analytical and experimental investigations to evaluate the effectiveness of strengthening W150x37 steel beams by

attaching GFRP laminates to their bottom and top flanges. The application of GFRP plates caused an approximate 78% increment in the peak moment limit of the steel beam. Lacki and Derlatka [27] investigated the impact of using polyurethane foam (PU) on the buckling characteristics of the I-beam made of Al6061-T6 and GFRP laminates. Four types of beams were analysed: (i) aluminium beam, (ii) aluminium-GFRP beam, (iii) aluminium-GFRP-PU beam, and (iv) aluminium-GFRP-PU-ribs beam. It was reported that PU reinforcement led to a 330% increment in the buckling resistance of the aluminium beam. Moreover, reinforcement with PU and ribs resulted in a 510% increase in buckling resistance of aluminium beam. On the other hand, the aluminium-GFRP beam exhibited a 45% higher load-bearing capacity compared to the aluminium beam. In another study of Lacki et al. [28], it was concluded that reinforcing the I-beam web with glass fibre-reinforced PU led to an approximate twofold enhancement in the buckling resistance of the aluminium beam.

Besides, various theoretical approaches have been proposed to estimate the LTB resistance of hybrid beams. Theoretical models commonly utilize energy principles or semi-analytical techniques to estimate the critical buckling load of structures [29]. Kabir and Seif [30] proposed an analytical model to predict the LTB resistance of steel I-beams reinforced with FRP sheets, while neglecting the influence of shear deformations. Girhammar and Pan [31] proposed an analytical solution to estimate the buckling resistance of two-layer members, but their study did not consider partial interaction between layers and shear deformations. Youssef [32] presented an analytical method to describe the nonlinear and linear characteristics of steel/FRP beams.

This study focuses on the finite element analysis (FEA) Al6061-T6 and Al6061-T6/CFRP hybrid I-beams. Although numerous numerical, theoretical, and experimental studies have investigated the buckling behaviour of FRPstrengthened I-beams, most have focused on general strengthening effects without thoroughly examining the critical parameters such as FRP thickness, fibre orientation angle, FRP length, and FRP location. To close this gap in the literature, this study systematically explores the influences of CFRP laminate thickness, fibre orientation angle, CFRP laminate length, and CFRP laminate location on the LTB behaviour of I-beams. A further novelty of this work is the consideration of equal thickness conditions between the CFRP-strengthened and un-strengthened I-beams, which allows for a more direct and meaningful comparison of structural performance. For all hybrid I-beam configurations, the web and flange thicknesses were kept equal to those of the aluminium (Reference) I-beam. Abaqus/Standard software was utilized to develop finite element (FE) models of aluminium and aluminium/CFRP hybrid I-beams. The FE model for aluminium I-beam was verified by comparison of the numerical findings with test data reported in the Ref. [5]

2 Finite element modelling

In the present work, FEA of Al6061-T6 and Al6061-T6/CFRP hybrid I-beams were conducted using

Abaqus/Standard software. The hybrid I-beams were created by attaching the CFRP laminates either to the web or to the flanges. Figure 1 and Table 1 detail the aluminium and aluminium/CFRP hybrid I-beams analysed in the current work. Reference (aluminium) beam was modelled based on the geometry (6061-4-A/B) presented by Wang et al. [5]. In specimens Beam 1 to 8, the aluminium I-beams were retrofitted by adhesively bonding CFRP plates to the web. It is important to highlight that in specimens Beam 1 to 8, web thickness was kept equal to that of the Reference beam. The length of all web-retrofitted I-beams (L_b) was consistently set to 1050 mm, identical to that of the Reference beam. The effect of CFRP plate thickness on LTB behaviour was assessed by analysing Beams 1 to 3. For this purpose, 0.5 mm (2-layered), 0.75 mm (3-layered), and 1.00 mm (4layered) CFRP plates with the fibre orientation of 0° (oriented along the length of the beam) were bonded to the web of the aluminium I-beam. Similarly, the influence of fibre orientation angle ([0°]4, [45°]4, and [90°]4) on LTB behaviour was evaluated through the comparison of Beams 3, 4, and 5. Considering Beams 3, 6, and 7, the impact of the length of CFRP plates (Lw,CFRP) bonded to the web on the LTB behaviour was examined. In Beams 6 and 7, CFRP plates with a length of 787.5 mm and 525 mm were bonded to the centre of the web along the aluminium I-beam's primary axis. Lastly, considering Beams 7 and 8, the effect of CFRP plate location on the LTB behaviour was investigated. In Beam 8, CFRP plates with the length of 262.5 mm were bonded to both ends of the web. The total length of the bonded CFRP plates for Beams 7 and 8 is identical to avoid the influence of CFRP plate length on LTB characteristic. The same procedure was followed for the beams hybridised by attaching CFRP plates to the flange. However, in this case, CFRP plates with thicknesses of 1.00 mm (4-layered), 2 mm (8-layered), and 3 mm (12-layered), all with 0° fibre orientation, were bonded to the flanges to determine the impact of CFRP plate thickness on the LTB characteristic. Additionally, the adhesive layer thickness is 0.1 mm for all aluminium/CFRP hybrid I-beams. The geometric configurations of aluminium and aluminium/CFRP hybrid I-beams are illustrated in Figure 2.

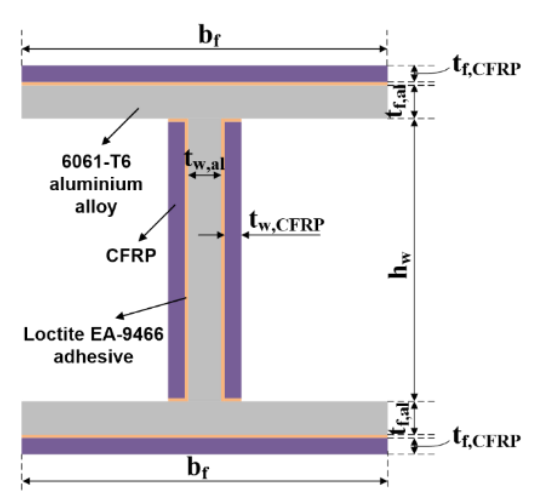


Figure 1. Schematic of cross-section of modelled I-beams

Table 1. Dimensions of the beam samples analysed	Table 1.	. Dimens	ions of t	the beam	samples	analysed
---	----------	----------	-----------	----------	---------	----------

Specimen	$b_{\mathrm{f}}\left(mm\right)$	$h_{\mathrm{w}}\left(mm\right)$	$t_{f,al}\left(mm\right)$	$t_{\text{f,CFRP}}\left(mm\right)$	$t_{\text{w,al}}(mm)$	$t_{\text{w,CFRP}}(mm)$	$L_{b}\left(mm\right)$	$L_{\text{f,CFRP}}(\text{mm})$	$L_{\text{w,CFRP}}(\text{mm})$	Fibre orientation (°)
Reference	17.85	92.13	3.94		2.85		1050			
Beam 1	17.85	92.13	3.94		1.65	0.50	1050		1050	$[0^{\circ}]_2$
Beam 2	17.85	92.13	3.94		1.15	0.75	1050		1050	$[0^{\circ}]_{3}$
Beam 3	17.85	92.13	3.94		0.65	1.00	1050		1050	[0°] ₄
Beam 4	17.85	92.13	3.94		0.65	1.00	1050		1050	[45°] ₄
Beam 5	17.85	92.13	3.94		0.65	1.00	1050		1050	[90°] ₄
Beam 6	17.85	92.13	3.94		0.65	1.00	1050		787.5	[0°] ₄
Beam 7	17.85	92.13	3.94		0.65	1.00	1050		525	[0°] ₄
Beam 8	17.85	92.13	3.94		0.65	1.00	1050		262.5	[0°] ₄
Beam 9	17.85	92.13	2.84	1.00	2.85		1050	1050		[0°] ₄
Beam 10	17.85	92.13	1.84	2.00	2.85		1050	1050		[0°] ₈
Beam 11	17.85	92.13	0.84	3.00	2.85		1050	1050		[0°] ₁₂
Beam 12	17.85	92.13	2.84	1.00	2.85		1050	1050		[45°] ₄
Beam 13	17.85	92.13	2.84	1.00	2.85		1050	1050		[90°] ₄
Beam 14	17.85	92.13	2.84	1.00	2.85		1050	787.5		[0°] ₄
Beam 15	17.85	92.13	2.84	1.00	2.85		1050	525		[0°] ₄
Beam 16	17.85	92.13	2.84	1.00	2.85		1050	262.5		[0°] ₄

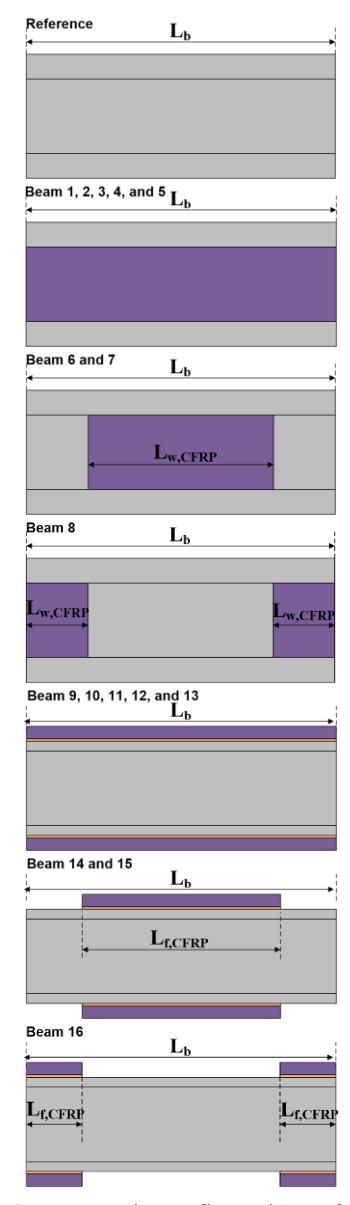


Figure 2. Geometric configurations of I-beams

In the context of buckling analysis, finite element methods can be generally categorized into two classes: the linear eigenvalue method, which estimates the critical instability load by calculating an eigenvalue problem, and the nonlinear incremental method, such as the arc-length technique, which accounts for geometric nonlinearities [29]. In the current work, linear eigenvalue and nonlinear analyses were conducted on aluminium and aluminium/CFRP hybrid I-beams. The Subspace Eigensolver in Abaqus was used to perform linear eigenvalue analyses in order to determine the critical LTB loads and associated mode shapes of aluminium and aluminium/CFRP hybrid I-beams. The first LTB mode shape obtained from linear eigenvalue analyses was considered as an initial geometrical imperfection. As suggested by Wang et al. [5], an initial geometrical imperfection with a peak magnitude of L_b/1000 was incorporated into each model. Furthermore, because of their low levels, residual stresses were not taken into account in the analyses.

2.1 Geometrical and material modelling

In this study, 3-D finite element modelling was performed utilizing Abaqus/Standard software. The 3-D geometry of the I-beam (representatively Beam 9) is illustrated in Figure 3. In all aluminium/CFRP hybrid models, the thickness of each CFRP lamina is 0.25 mm.

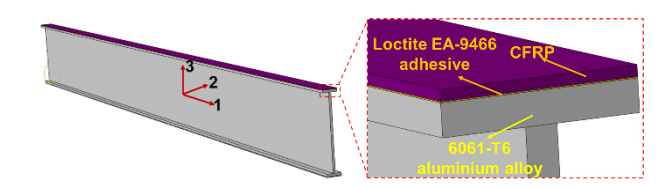


Figure 3. 3-D geometry of I beam

An elastic-perfectly plastic material model was employed to simulate the mechanical characteristics of the 6061-T6 aluminium alloy. As illustrated in Figure 4, the elastic-perfectly plastic material model accurately captures the material behaviour of Al6061-T6. Mechanical properties of Al6061-T6 are listed in Table 2.

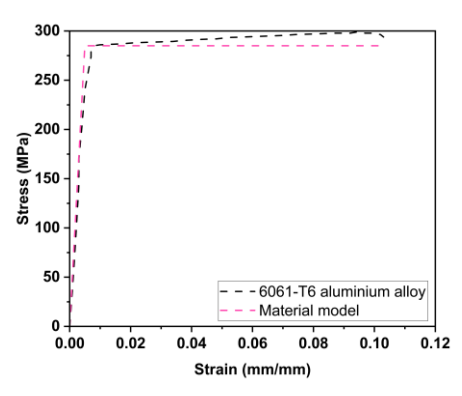


Figure 4. Stress-strain curve of 6061-T6 aluminium alloy [5] and material model

Table 2. Mechanical features of Al6061-T6 used in analyses [5]

Properties	Value
Young's modulus (GPa)	57.5
Yield strength (MPa)	285
Poisson's ratio	0.3

The mechanical behaviour of the CFRP plate was simulated utilizing the orthotropic linear elastic material model. Some mechanical features of the CFRP lamina presented in Table 3 were taken from the study reported by Wong et al [33].

Table 3. Mechanical properties of CFRP lamina [33]

1 1	
Properties	Value
Young's modulus in fibre direction (E ₁) (GPa)	131.9
Young's modulus in transverse direction (E ₂) (GPa)	9.51
Young's modulus through thickness (E ₃) (GPa)	9.43
Poisson's ratio (v_{12})	0.326
(v_{13})	0.341
(v_{23})	0.485
Shear modulus in fibre plane (G_{12}) (GPa)	5.27
Shear modulus through thickness $(1-3 \text{ plane}) (G_{13}) (GPa)$	7.03
Shear modulus through thickness (2-3 plane) (G ₂₃) (GPa)	3.39
Tensile strength in fibre direction (X_T) (MPa)	1328
Compressive strength in fibre direction (X_C) (MPa)	1064
Tensile strength in transverse direction (Y _T) (MPa)	70.9
Compressive strength in transverse direction (Y_C) (MPa)	221
Shear strength in fibre direction (S _L) (MPa)	71.2
Shear strength in transverse direction (S_T) (MPa)	94.5
Compressive fracture energy of matrix (N/mm)	0.33
Tensile fracture energy of matrix (N/mm)	0.33
Compressive fracture energy of fibre (N/mm)	2
Tensile fracture energy of fibre (N/mm)	2

Hashin's theory [34] for the damage initiation criterion of CFRP composite was employed. This theory considers four distinct failure modes: tensile and compressive fibre failure and tensile and compressive matrix failure. Damage initiation for each failure mode occurs when the corresponding criterion, as defined by Equations (1)-(4), is satisfied. In these equations, α denotes the shear stress contribution coefficient. $\widehat{\sigma}_{11}$, $\widehat{\sigma}_{22}$, and $\widehat{\tau}_{12}$ are the stress tensor components [35]. A linear softening law is employed to characterize the damage evolution.

Fibre tension
$$\left(\widehat{\sigma_{11}} \ge 0\right)$$
: $\left(\frac{\widehat{\sigma_{11}}}{X_T}\right)^2 + \alpha \left(\frac{\widehat{\tau_{12}}}{S_L}\right)^2 \ge 1$ (1)

Fibre compression
$$(\sigma_{11} < 0)$$
: $\left(\frac{\widehat{\sigma_{11}}}{X_C}\right)^2 \ge 1$ (2)

Matrix tension
$$(\sigma_{22} \ge 0)$$
: $(\frac{\widehat{\sigma_{22}}}{Y_T})^2 + (\frac{\widehat{\tau_{12}}}{S_L})^2 \ge 1$ (3)

Matrix compression
$$\left(\frac{\widehat{\sigma_{22}}}{2S_T}\right)^2 + \left[\left(\frac{Y_C}{2S_T}\right)^2 - 1\right]\left(\frac{\widehat{\sigma_{22}}}{Y_C}\right) + \left(\frac{\widehat{\tau_{12}}}{S_L}\right)^2 \ge 1$$
 (4)

Loctite EA-9466 epoxy adhesive was selected as an adhesive for glueing CFRP to 6061-T6 aluminium alloy. The adhesive was modelled as a linear elastic material. The epoxy adhesive's performance was evaluated utilizing the Cohesive Zone Model (CZM) integrated into Abaqus/Standard. A bilinear traction-separation law was used. The damage initiation was modelled using the quadratic nominal stress criteria (QUADS). Damage initiation occurs when the Equation (5) was satisfied [35]. In Equation (5) t_s^0 , t_n^0 , and t_t^0 represent the maximum nominal stresses in the first shear, normal, and second shear directions, respectively. Correspondingly, t_n , t_s , and t_t denote the predicted stresses in these directions. The Macaulay bracket, (), signifies that compressive stresses don't trigger damage [36]. Damage evolution in the adhesive is predicted using the energy-based Benzeggagh-Kenane (BK) criterion. More detailed information about cohesive zone modelling can be found in the study conducted by Taş [37]. The mechanical features of Loctite EA-9466 are illustrated in Table 4. In this work, ultimate tensile strength and shear strength were considered as maximum nominal stress at normal direction and first shear direction, respectively. Moreover, the nominal stresses and critical fracture energies are assumed to be equal in the first and second shear directions.

$$\left\{\frac{\langle t_n \rangle}{t_n^0}\right\}^2 + \left\{\frac{t_s}{t_s^0}\right\}^2 + \left\{\frac{t_t}{t_t^0}\right\}^2 = 1 \tag{5}$$

Table 4. Mechanical properties of Loctite EA-9466 lamina [38]

Properties	Value
Elasticity modulus (E) (GPa)	1.91
Poisson's ratio (υ)	0.35
Yield strength (σ_Y) (MPa)	41.33
Tensile strength (σ_u) (MPa)	44.38
Shear strength (τ) (MPa)	13.98
Fracture strain (ε_f) (%)	3.8582
Mode I critical strain energy release rate (G_{IC}) (N/mm)	0.313
Mode II critical strain energy release rate (G_{IIC}) (N/mm)	0.155

2.2. Meshing and boundary conditions

The constructed mesh of the I-beam (exemplified by Beam 9) is presented in Figure 5. The mesh of the aluminium alloy component was constructed using 8-node linear hexahedral elements (C3D8R). The aluminium alloy component has an element size of 5 mm along its length and web height, and 1.5 mm along flange width, flange thickness, and web thickness. 8-node first order reduced integration

quadrilateral continuum shell elements (SC8R) were used to mesh the CFRP component. The CFRP component was discretized through its thickness into a number of elements equivalent to the lamina number. Furthermore, the finite element mesh size for the CFRP laminate bonded to the I-beam's flange is set to 5 mm along its length and 1.5 mm along its width. For the CFRP plate glued to the I-beam's web, the element size along its height is set to 5 mm. The adhesive layer was discretized using 8-node 3-D cohesive elements (COH3D8). A single layer of cohesive elements was employed through the thickness of the adhesive layer. The element numbers for all I-beam types are detailed in Table 5. Depending on the I-beam configuration, the total number of elements ranges from 22680 to 78120.

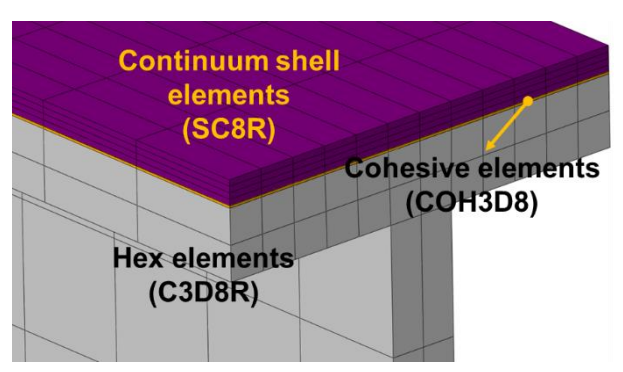


Figure 5. The constructed mesh

Table 5. Number of elements for all types of I-beams

Cmaaimam	Components			Total
Specimen -	Aluminium alloy	CFRP	Adhesive	Total
Reference	22680			22680
Beam 1	23100	15120	8400	46620
Beam 2	23100	22680	8400	54180
Beam 3	23100	30240	8400	61740
Beam 4	23100	30240	8400	61740
Beam 5	23100	30240	8400	61740
Beam 6	23100	22752	6320	52172
Beam 7	23210	15120	4200	42530
Beam 8	23210	15264	4240	42714
Beam 9	17640	20160	5040	42840
Beam 10	12600	40320	5040	57960
Beam 11	12600	60480	5040	78120
Beam 12	17640	20160	5040	42840
Beam 13	17640	20160	5040	42840
Beam 14	17640	15168	3792	36600
Beam 15	17724	10080	2520	30324
Beam 16	17724	10176	2544	30444

The mesh sensitivity analysis was carried out for the Reference beam. LTB analyses were performed using two different mesh densities: one with a total of 335160 elements and another with 22680 elements. The corresponding M_{cr} values obtained were 0.636 kNm and 0.615 kNm, respectively. This represents a deviation of approximately 3.3%, indicating that the numerical results are sufficiently mesh independent.

The boundary conditions for each I-beam were applied through reference points (RPs) located at the shear centre of both ends of the I-beam. All degrees of freedom of the RPs were tied to the end surfaces of I-beams by utilizing rigid body constraints in Abaqus/Standard software. At one end,

all translational and rotational movements were restrained, except for rotation about the y-axis. At the opposite end, the beam is subjected to identical boundary conditions, except it is free to translate along the x-axis. As for the loading conditions, the bending moment (M_y) to each reference point was applied to induce pure bending conditions. In linear eigenvalue analysis, a bending moment of 1 Nmm was applied. However, in the subsequent nonlinear analysis, the critical LTB bending moment, obtained from linear eigenvalue analysis, was applied as the bending moment. Figure 6 illustrates the applied boundary conditions.

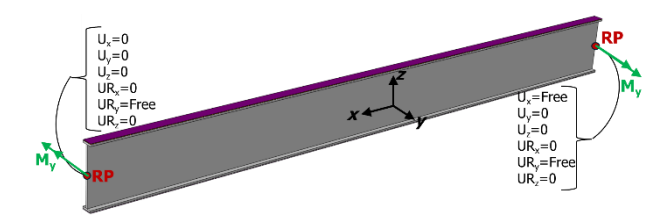


Figure 6. Boundary conditions

2.3. Verification of the finite element model

The verification of the finite element model was carried out by comparing the FEA findings with the test data reported by Wang et al. [5]. The Reference beam (refer to Table 1), designated as 6061-4-A/B by Wang et al. [5], was modelled according to the geometric configuration and material properties reported in their work. A strong conformity was seen between the experimental and numerical findings. The experimental elastic critical LTB bending moment (M_{cr}) was reported as 0.636 kNm. FEA predicted a corresponding value of 0.615 kNm, resulting in a 3.3% relative error between the numerical and test findings. Moreover, the comparison of numerical and experimental results concerning moment-rotation curves is illustrated in Figure 7. Wang et al. [5] normalized the pure bending moment M with respect to the elastic bending capacity $M_{0.2}$. $M_{0.2}$ is equal to the product of the material's yield strength and the elastic section modulus of the gross section. Thus, $M/M_{0.2}$ denotes the lateral-torsional stability factor. According to Figure 7, FEM accurately captures the moment-rotation relationship. Therefore, it can be concluded that FEA is an effective method for accurately forecasting the LTB behaviour of I-beams.

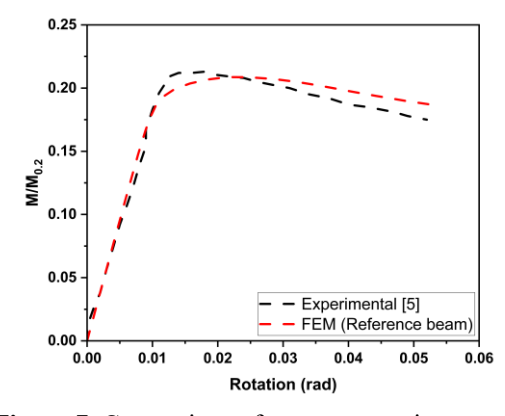


Figure 7. Comparison of moment-rotation curves

3 Results and discussion

3.1 Effect of CFRP laminate thickness

The influence of the thickness of the CFRP plate on the LTB resistance of I-beams was examined by bonding laminates of varying thicknesses to either the web or flange. Specifically, CFRP laminates with thicknesses of 0.5 mm, 0.75 mm, and 1.0 mm were bonded to the web, while laminates of 1.0 mm, 2.0 mm, and 3.0 mm were applied to the flange. Table 6, reflecting the effect of CFRP laminate thickness, presents the elastic critical LTB bending moments (M_{cr}) .

Table 6. The effect of CFRP plate thickness on M_{cr}

Specimen	M_{cr} (kNm)	Change (%)		
Reference	0.615			
	CFRP plate bonde	ed to web		
Beam 1	0.522	-15.1		
Beam 2	0.542	-11.9		
Beam 3	0.563	-8.5		
CFRP plate bonded to flange				
Beam 9	0.685	11.4		
Beam 10	0.783	27.3		
Beam 11	0.907	47.5		

It is evident that, based on the CFRP laminate thickness, glueing CFRP plates to the web of the I-beam (while maintaining the web thickness equivalent to that of the Reference beam) resulted in a reduction in the M_{cr} value ranging from 8.5% to 15.1% in comparison to the Reference beam. This may be explained by the lower torsional stiffness of the CFRP plate relative to that of the Al6061-T6. Furthermore, local interaction effects at the web-flange junction may have some influence on M_{cr} . However, this effect is considered to be negligible when compared to the dominant influence of reduced torsional stiffness. Moreover, increasing the thickness of the CFRP laminate bonded to the web led to a corresponding enhancement in the M_{cr} . It is critical to emphasize that as the CFRP plate thickness increased, the thickness of Al6061-T6 in the web correspondingly decreased. While the reduction in aluminium thickness lowers the overall torsional stiffness, the concurrent increase in CFRP thickness contributes more significantly to torsional stiffness. Thus, the net effect is an enhancement in M_{cr} .

Conversely, glueing CFRP laminates to the flanges significantly enhanced the resistance to LTB. Based on the CFRP laminate thickness, M_{cr} value increased by approximately 11.4% to 47.5% in comparison to the Reference beam. During LTB, the flanges tend to move in the lateral direction, causing the beam to bend about its weak axis. A higher stiffness in the longitudinal direction improves resistance to such lateral displacement. As CFRP laminates exhibit greater rigidity than 6061-T6 aluminium alloy, their application to the flanges substantially increases the longitudinal-axis stiffness of the beam, thereby enhancing its M_{cr} . Furthermore, an increase in CFRP laminate thickness resulted in an increase in M_{cr} , which can be attributed to the enhanced flexural rigidity provided by the thicker laminates. Pham et al. [20] also studied the influence of GFRP laminate thickness on the buckling strength of a steel I-beam. In their study, the GFRP laminates were glued to the I-beams' compression flanges. The findings demonstrated that instability load increased with the increase of GFRP laminate thickness. Notably, a maximum improvement of 94.4% in buckling strength was observed when a 30 mm thick GFRP plate was applied to the compression flange.

Figure 8 presents moment-rotation curves obtained from nonlinear analyses, illustrating the influence of CFRP laminate thickness. The moment-rotation curve of the Reference beam shows linear behaviour up to the yield point. Beyond the yield point, the moment remains nearly constant (increase is very slow) despite increasing rotation. Once the rotation reaches 0.0214 rad, the moment-rotation curve exhibits a descending trend. Beam 1, 2, and 3 exhibits similar moment-rotation characteristics to that of the Reference beam. A rise in the thickness of the CFRP laminate bonded to the web resulted in a steeper slope in the linear section of the moment-rotation curve. Moreover, glueing the CFRP laminate to the web delayed the onset of LTB, occurring at rotation angles of 0.0237 rad for Beam 1, 0.0243 rad for Beam 2, and 0.0240 rad for Beam 3. On the other hand, moment-rotation curves of Beam 9, 10, and 11 slightly differ from that of the Reference beam. Notably, the rise in moment beyond the yield point with increasing rotation is more pronounced in these beams. Attaching the CFRP plate to the flange also delayed the initiation of LTB, occurring at rotation angles of 0.0320 rad for Beam 9, 0.0370 rad for Beam 10, and 0.0388 rad for Beam 11.

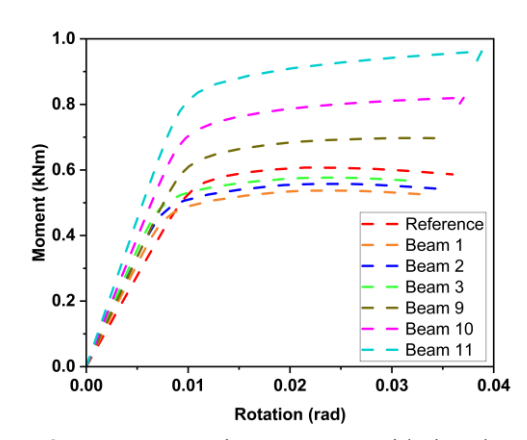


Figure 8. Moment-rotation curves considering the effect of CFRP laminate thickness

Figure A1 in the Appendix illustrates the von-Mises stress distribution for aluminium alloy component of I-beams, contour of fibre compression damage initiation criterion (HSNFCCRT) for CFRP component of I-beams, and the contour of overall scalar stiffness degradation (SDEG) for adhesive component of I-beams, all evaluated at the moment of M_{cr} . Damage initiation criterion (HSNFCCRT) is satisfied if its value reaches 1. Once damage initiation occurs, further loading leads to a degradation of material stiffness. The SDEG value of 1 represents the complete failure of the adhesive. However, in the current work, the maximum SDEG value is limited to 0.97.

An examination of von Mises stress distributions for aluminium alloy components of Reference beam and Beams 1, 2, 3, 9, 10, and 11 revealed that the aluminium alloy underwent plastic deformation, as the maximum von Mises stress reached the yield strength of the aluminium alloy. As for the CFRP component, the values of HSNFCCRT indicated that no fibre compression damage initiation occurred for Beam 1, 2, and 3. On the other hand, for Beam 9, the HSNFCCRT value of 0.844 suggested that fibre compression damage initiation was imminent. For Beams 10 and 11, the HSNFCCRT value of 1 confirmed the onset of damage in the CFRP component. According to the contours of SDEGs, no complete failure occurred at the adhesive layer of Beams 1, 2, 3, 9, 10, and 11.

When CFRP laminates were bonded to the web, variations in the laminate thickness did not significantly affect the von-Mises stress distribution, the HSNFCCRT contour, or the SDEG contour. However, when CFRP laminates were bonded to the flange, damage initiation occurred at the CFRP plates as the thickness of the CFRP laminates increased. Moreover, although complete adhesive failure did not occur, thicker laminates led to higher SDEG values.

3.2 Effect of fibre orientation angle

The impact of fibre alignment angle on the LTB resistance of I-beams was analysed by bonding 1 mm thick CFRP laminates with fibre orientation angles of $[0^{\circ}]_4$, $[45^{\circ}]_4$, and $[90^{\circ}]_4$ to either the web or flange. Table 7, illustrating the influence of fibre orientation angle, shows the M_{cr} values.

Regardless of whether the CFRP laminates are bonded to the web or flange, the fibre orientation angle substantially influenced the M_{cr} . For I-beams with CFRP laminates bonded to their webs, the M_{cr} rose with the increase of fibre orientation angle up to a certain angle, beyond which further increments in the fibre alignment angle caused a reduction in the M_{cr} . Increasing the fibre alignment angle from 0° to 45° resulted in a 5.3% increase in M_{cr} value. Despite this increase, the M_{cr} value for the Beam 4 is still 3.6% lower than the M_{cr} value for the Reference beam. On the other hand, increasing the fibre orientation angle from 0° to 90° led to a 2.1% reduction in M_{cr} value. When fibres are aligned along the longitudinal axis (0°) or transverse axis (90°), FRP laminates provide low resistance to torsion. However, FRP laminates with 45° fibre orientation angle have higher torsional stiffness due to the shear-resisting nature of these fibre orientations. This enhanced torsional stiffness results in an increased M_{cr} . Soltani [39] examined the effect of fibre orientation angle in the web on the lateral buckling response of simply supported laminated I-beams. The flanges were modelled as unidirectional laminates with a [0°]₁₆ stacking sequence, while the web was assumed to consist of a symmetric angle-ply laminate with a $[\pm \theta^{\circ}]_{4S}$ configuration. Similarly, the findings indicated that the lateral buckling capacity increases as the fibre angle is rotated off-axis, reaching its maximum at θ =45°, and subsequently decreases sharply, attaining a minimum at θ =90°.

For I-beams with CFRP laminates bonded to their flanges, M_{cr} diminished with the increase of fibre alignment

angle. Increasing the fibre alignment angle from 0° to 45° and from 0° to 90° led to reductions of 24.5% and 30.0% in M_{cr} values, respectively. Increasing the fibre orientation angle caused the M_{cr} values for the hybridised beams (Beam 12 and Beam 13) to be lower than the M_{cr} value for the Reference beam. Reductions in M_{cr} values are 15.9% and 22.1% for Beam 12 and 13, respectively. As discussed previously, during the LTB, flanges of an I-beam bend about their weak axis. As the fibre orientation angle increases, flexural rigidity in the longitudinal direction diminishes, causing a reduced resistance to lateral displacement. This reduced resistance to lateral movement results in a decreased M_{cr} .

Table 7. The effect of fibre orientation angle on M_{cr}

		•		
Specimen	M _{cr} (kNm)	Change (%)		
Reference	0.615			
	CFRP plate bonded	l to web		
Beam 3	0.563	-8.5		
Beam 4	0.593	-3.6		
Beam 5	0.551	-10.4		
CFRP plate bonded to flange				
Beam 9	0.685	11.4		
Beam 12	0.517	-15.9		
Beam 13	0.479	-22.1		

Figure 9 displays the moment-rotation curves obtained from nonlinear analyses, highlighting the influence of fibre alignment angle. In general, the fibre orientation angle does not have a considerable impact on the moment-rotation characteristics of the aluminium/CFRP hybrid I-beams. For the Beams 3, 4, and 5, LTB occurred at 0.0240 rad, 0.0226 rad, and 0.0234 rad rotation angles, respectively. These results suggested that glueing the CFRP laminates to the web with a fibre orientation angle of 45° induced an early LTB failure. Additionally, for the I-beams hybridised by attaching the CFRP laminates to the web, a decrease in the fibre orientation angle resulted in a steeper slope in the linear portion of the moment-rotation curve. As for the Beams 9, 12, and 13, LTB occurred at 0.0320 rad, 0.0220 rad, and 0.0235 rad rotation angles, respectively. This trend indicated that, when the CFRP laminates were bonded to the flanges, a lower fibre orientation angle contributed to delaying the onset of LTB. Furthermore, a decrease in fibre orientation angle resulted in an increased initial stiffness, as reflected by the steeper linear response in the moment-rotation curves.

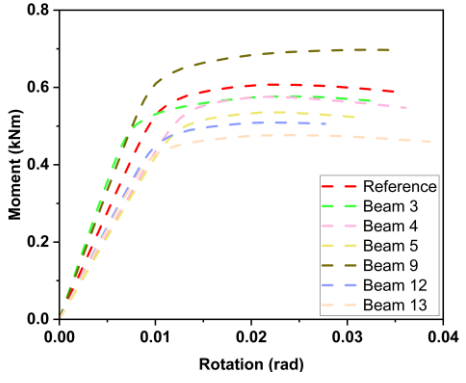


Figure 9. Moment-rotation curves considering the effect of fibre orientation angle

An examination of Figure A1 revealed that changes in the fibre alignment angle had a negligible impact on the von Mises stress distribution, as well as on the HSNFCCRT and SDEG contours for the I-beams hybridised by glueing the CFRP laminates to the web. Although the aluminium alloy underwent plastic deformation, the HSNFCCRT and SDEG values confirmed that fibre compression damage initiation in the CFRP laminate and complete failure in the adhesive layer did not occur. The same behaviour was observed for I-beams hybridized by glueing the CFRP laminates to the flanges.

3.3 Effect of CFRP laminate length

The impact of CFRP laminate length on the LTB behaviour of I-beams was investigated by attaching CFRP laminates of 1050 mm, 787.5 mm (about 75% of span length), and 525 mm (about 50% of span length) in length either to the web or the flange. Table 8 presents the M_{cr} values corresponding to different CFRP laminate lengths.

The M_{cr} was negatively affected by a reduction in the length of CFRP laminates, irrespective of whether they were bonded to the web or flange of the I-beam. When the CFRP laminate length was reduced from 1050 mm to 787.5 mm, the M_{cr} values decreased by 3.2% for web-bonded configurations and by 16.6% for flange-bonded configurations. A further reduction in laminate length to 525 mm resulted in a 6.2% decrease in M_{cr} values for webbonded I-beams and an 18.9% decrease for flange-bonded Ibeams. These findings clearly demonstrated that the influence of CFRP laminate length on M_{cr} was significantly more pronounced for flange-bonded I-beams than webbonded I-beams. Lenwari et al. [40] also studied the influence of the length of the CFRP plate bonded to the steel I-beam's bottom flange on the flexural performance. CFRP plate lengths were 0.50 m, 0.65 m, and 1.20 m, while the span length was 1.80 m. The study similarly concluded that an increase in plate length led to a corresponding increase in the failure load.

Table 8. The effect of CFRP laminate length on M_{cr}

Specimen	M _{cr} (kNm)	Change (%)
Reference	0.615	
	CFRP plate bonded	to web
Beam 3	0.563	-8.5
Beam 6	0.545	-11.4
Beam 7	0.528	-14.1
	CFRP plate bonded to	to flange
Beam 9	0.685	11.4
Beam 14	0.571	-7.2
Beam 15	0.555	-9.8

Figure 10 illustrates the moment–rotation curves obtained from nonlinear analyses, emphasizing the impact of CFRP plate length. Overall, the length of the CFRP plate exhibited a negligible impact on the moment-rotation characteristic of the aluminium/CFRP hybrid I-beams. However, regardless of whether CFRP laminate bonded to the web or the flange, an increase in CFRP laminate length led to a noticeable enhancement in initial stiffness, as evidenced by a steeper slope in the linear portion of the moment–rotation curves. Beams 3, 6, and 7 experienced LTB at rotation angles of 0.0240 rad, 0.0230 rad, and 0.0211

rad, respectively. Similarly, Beams 9, 14, and 15 exhibited LTB at rotation angles of 0.0320 rad, 0.0222 rad, and 0.0224 rad, respectively. These findings suggest that increasing the length of the CFRP laminate effectively delays the LTB onset.

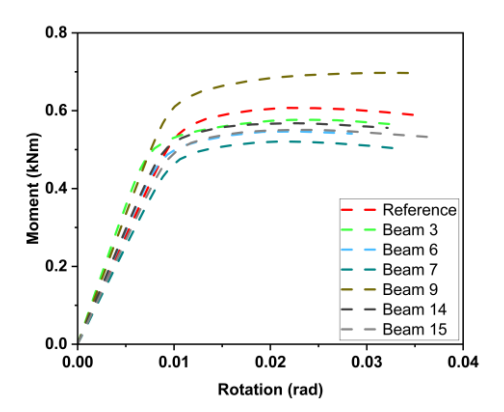


Figure 10. Moment-rotation curves considering the effect of CFRP laminate length

An examination of Figure A1 demonstrated that impact of the length of the CFRP laminate on the failure modes of the components of I-beams differed for the web-bonded Ibeams and flange-bonded I-beams. In web-bonded I-beams, the HSNFCCRT contours indicated that the initiation of fibre compression damage in the CFRP laminate remained unaffected by variations in CFRP laminate length. Furthermore, while SDEG values increased with decreasing CFRP laminate length, complete adhesive layer failure was not observed. Conversely, in flange-bonded I-beams, the maximum HSNFCCRT values diminished with decreasing laminate length, indicating the absence of fibre compression damage initiation. However, a shorter CFRP laminate led to complete adhesive failure at the adhesive ends. This phenomenon is attributed to high stress concentrationsincluding transverse shear, peeling, longitudinal normal, and lateral normal stresses-at the adhesive ends, which become more pronounced as the CFRP laminate length decreases [41]. Lenwari et al. [40] also reported that bonding a short CFRP laminate to the bottom flange of a steel I-beam primarily resulted in plate debonding failure, whereas applying a longer CFRP plate to the same location led to FRP rupture failure

3.4 Effect of CFRP laminate location

The influence of CFRP laminate location on the LTB resistance of the I-beams was investigated by bonding CFRP laminates of 262.5 mm length to both ends of either web or flange of the I-beam and 525 mm length to the midspan of either web or flange of I-beam. Table 9 summarizes the M_{cr} values, highlighting the influence of CFRP laminate location on LTB resistance.

The influence of CFRP laminate location on M_{cr} is more significant in web-bonded I-beams compared to flange-bonded I-beams. In the case of web-bonded configurations, positioning 262.5 mm length CFRP laminates to both ends of the I-beam resulted in an 11.2% reduction in M_{cr} value

compared to the I-beams with a 525 mm length CFRP laminate bonded to the midspan. Conversely, for flange-bonded I-beams, the location of the CFRP laminate exhibited negligible influence on M_{cr} .

Table 9. The effect of CFRP laminate location on M_{cr}

Specimen	M_{cr} (kNm)	Change (%)
Reference	0.615	
	CFRP plate bonde	ed to web
Beam 7	0.528	-14.1
Beam 8	0.469	-23.7
	CFRP plate bonded	l to flange
Beam 15	0.555	-9.8
Beam 16	0.554	-9.9

Figure 11 shows the moment–rotation curves obtained from nonlinear analyses, with a focus on the impact of CFRP laminate location. The findings revealed that the position of the CFRP laminate had no discernible impact on the moment-rotation characteristics of both web-bonded and flange-bonded configurations. Furthermore, the slope of the initial linear segment of the moment–rotation curve remained unaffected by the position of the CFRP laminate. For the Beams 7 and 8, LTB occurred at 0.0211 rad and 0.0186 rad rotation angles, respectively. These results revealed that positioning the CFRP laminate to both ends of the web led to an early LTB failure. However, Beams 15 and 16 exhibited LTB at the same rotation angle of 0.0224 rad.

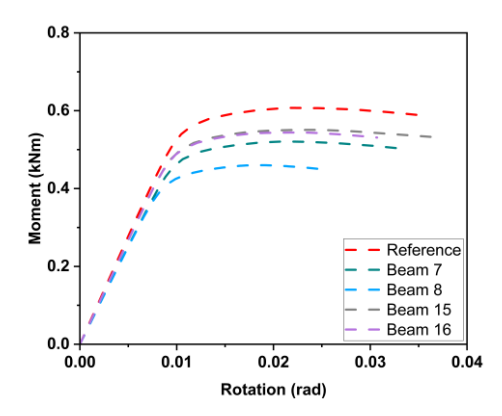


Figure 11. Moment-rotation curves considering the effect of CFRP laminate location

Analysing Figure A1 revealed that CFRP laminate location had a negligible influence on the HSNFCCRT contours of CFRP laminates for both web-bonded and flange-bonded I-beams. Low maximum HSNFCCRT values indicated no damage in the CFRP laminate. On the other hand, for web-bonded I-beams, positioning the CFRP laminate to both ends of the web caused a failure in the adhesive ends. This failure is more pronounced for flange-bonded I-beams.

4 Conclusion

According to the obtained results, the following conclusions are evident:

- FEA provides an accurate and robust method for predicting LTB behaviour of aluminium and aluminium/CFRP hybrid I-beams.
- The LTB behaviour of I-beams was strongly influenced by CFRP laminate thickness, fibre orientation angle, CFRP laminate length, and CFRP laminate location. However, the effect of these parameters differed for web-bonded and flangebonded I-beams.
- Overall, M_{cr} decreased when the CFRP laminate was bonded to the I-beam's web, compared to the Reference (aluminium) beam. However, when the CFRP laminate was bonded to the flange, its effect on M_{cr} could be either beneficial or detrimental, depending on the CFRP laminate thickness, fibre orientation angle, CFRP laminate length, and CFRP laminate location.
- Attaching a 3 mm-thick CFRP laminate with the fibre orientation angle of 0° to the flange of I-beam led to a 47.5% improvement in M_{cr} value when compared to the Reference beam.
- For the flange-bonded I-beams, as the fibre orientation angle increased, M_{cr} reduced. However, for the web-bonded I-beams, M_{cr} reached its maximum at a fibre orientation angle of 45°.
- As the length of the CFRP laminate decreased, M_{cr} declined for both web-bonded and flange-bonded I-beams. A reduction in CFRP laminate length from 1050 mm to 525 mm resulted in decreases in M_{cr} by 6.2% and 18.9% for web-bonded and flange-bonded configurations, respectively.
- The location of CFRP laminates significantly influenced the M_{cr} value for web-bonded I-beams, whereas it had a negligible effect in flange-bonded configurations.

Similarity rate (iThenticate): %16

References

- [1] D. Sonck and J. Belis, Elastic lateral-torsional buckling of glass beams with continuous lateral restraints. Glass Structures & Engineering, 1(1), 173–194, 2016. https://doi.org/10.1007/s40940-016-0023-4.
- [2] F. M. Mazzolani, Structural applications of aluminium in civil engineering. Structural Engineering International, 16(4), 280–285, 2006. https://doi.org/10.2749/101686606778995128.
- [3] B. R. Russell and A. P. Thrall, Portable and rapidly deployable bridges: Historical perspective and recent technology developments. Journal of Bridge Engineering, 18(10), 1074–1085, 2013. https://doi.org/10.1061/(ASCE)BE.1943-5592.0000454.
- [4] D. Skejić, M. Lukić, N. Buljan and H. Vido, Lateral torsional buckling of split aluminium mullion. Key Engineering Materials, 710, 445–450, 2016. https://doi.org/10.4028/www.scientific.net/KEM.710. 445.

- [5] Y. Q. Wang, H. X. Yuan, Y. J. Shi and M. Cheng, Lateral-torsional buckling resistance of aluminium Ibeams. Thin-Walled Structures, 50(1), 24–36, 2012. https://doi.org/10.1016/j.tws.2011.07.005.
- [6] X. Guo, Z. Xiong and Z. Shen, Flexural-torsional buckling behavior of aluminum alloy beams. Frontiers of Structural and Civil Engineering, 9(2), 163–175, 2015. https://doi.org/10.1007/s11709-014-0272-8.
- [7] C. Faella, F. M. Mazzolani, V. Piluso and G. Rizzano, Local buckling of aluminum members: Testing and classification. Journal of Structural Engineering, 126(3), 353–360, 2000. https://doi.org/10.1061/(AS CE)07339445(2000)126:3(353).
- [8] Y. Zhang, Y. Bu, Y. Wang, Z. Wang and Y. Ouyang, Study of flexural-torsional buckling behaviour of 6061-T6 aluminium alloy unequal-leg angle columns. Thin-Walled Structures, 164, 107821, 2021. https://doi.org/10.1016/j.tws.2021.107821.
- [9] Y. Q. Wang, Z. X. Wang, X. G. Hu, J. K. Han and H. J. Xing, Experimental study and parametric analysis on the stability behavior of 7A04 high-strength aluminum alloy angle columns under axial compression. Thin-Walled Structures, 108, 305–320, 2016. https://doi.org/10.1016/j.tws.2016.08.029.
- [10] Z. Xu, Y. Zhang, L. Zhang, Y. Chen and G. Tong, Experimental and numerical investigation of axially loaded aluminium alloy angle struts with lateral bracing on one leg. Thin-Walled Structures, 213, 113310, 2025. https://doi.org/10.1016/j.tws.2025.113310.
- [11] N. M. F. Silva, D. Camotim, N. Silvestre, J. R. Correia and F. A. Branco, First-order, buckling and postbuckling behaviour of GFRP pultruded beams. Part 2: Numerical simulation. Computers & Structures, 89(21– 22), 2065–2078, 2011. https://doi.org/10.1016/j.co mpstruc.2011.07.006.
- [12] J. R. Correia, F. A. Branco, N. M. F. Silva, D. Camotim and N. Silvestre, First-order, buckling and post-buckling behaviour of GFRP pultruded beams. Part 1: Experimental study. Computers & Structures, 89(21–22), 2052–2064, 2011. https://doi.org/10.1016/j.compstruc.2011.07.005.
- [13] J. T. Mottram, Lateral-torsional buckling of a pultruded I-beam. Composites, 23(2), 81–92, 1992. https://doi.org/10.1016/0010-4361(92)90108-7.
- [14] J. F. Davalos and P. Qiao, Analytical and experimental study of lateral and distortional buckling of FRP wideflange beams. Journal of Composites for Construction, 1(4), 150–159, 1997. https://doi.org/10.10 61/(ASCE)10900268(1997)1:4(150).
- [15] G. J. Turvey, Effects of load position on the lateral buckling response of pultruded GRP cantilevers Comparisons between theory and experiment. Composite Structures, 35(1), 33–47, 1996. https://doi.org/10.1016/0263-8223(96)00022-0.
- [16] P. Qiao, G. Zou and J. F. Davalos, Flexural–torsional buckling of fiber-reinforced plastic composite cantilever I-beams. Composite Structures, 60(2), 205–217, 2003. https://doi.org/10.1016/S02638223(02)00304-5.

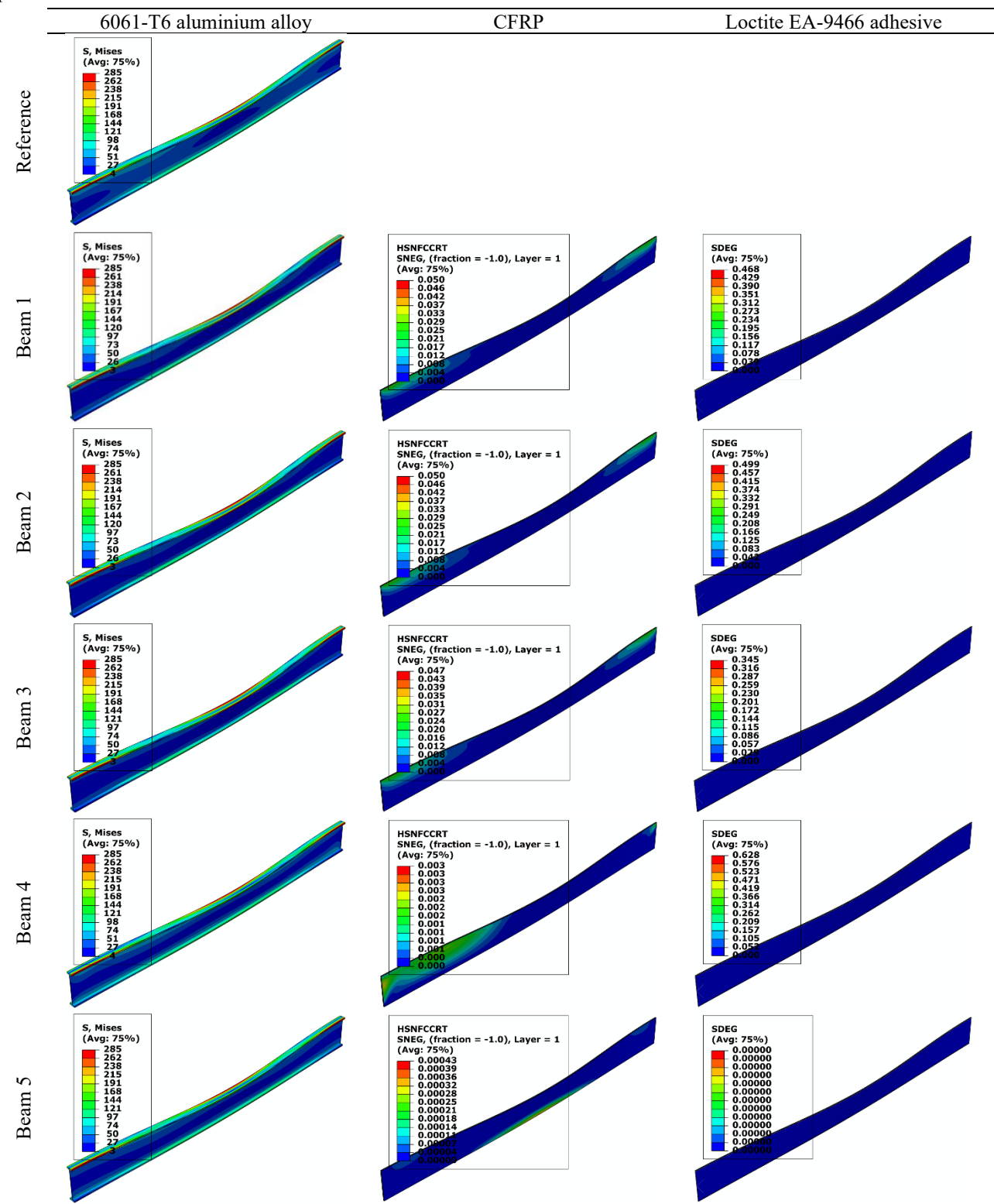
- [17] J. Lee, S.-E. Kim and K. Hong, Lateral buckling of I-section composite beams. Engineering Structures, 24(7), 955–964, 2002. https://doi.org/10.1016/S0141-0296(02)00016-0.
- [18] V. Kahya, Buckling analysis of laminated composite and sandwich beams by the finite element method. Composites Part B: Engineering, 91, 126–134, 2016. https://doi.org/10.1016/j.compositesb.2016.01.031.
- [19] E. J. Barbero and I. G. Raftoyiannis, Local buckling of FRP beams and columns. Journal of Materials in Civil Engineering, 5(3), 339–355, 1993. https://doi.org/10.1061/(ASCE)08991561(1993)5:3(339).
- [20] P. Van Pham, M. Mohareb and A. Fam, Lateral torsional buckling of steel beams strengthened with GFRP plate. Thin-Walled Structures, 131, 55–75, 2018. https://doi.org/10.1016/j.tws.2018.06.025.
- [21] P. Van Pham, An innovated theory and closed form solutions for the elastic lateral torsional buckling analysis of steel beams/columns strengthened with symmetrically balanced GFRP laminates. Engineering Structures, 256, 114046, 2022. https://doi.org/10.10 16/j.engstruct.2022.114046.
- [22] P. Van. Pham, Enhancement of moment resistance of steel beams with initial imperfections and residual stresses by using stiffeners and GFRP plates. Journal of Materials and Engineering Structures, 7(4), Article 4, 2020.
- [23] E. Ghafoori and M. Motavalli, Lateral-torsional buckling of steel I-beams retrofitted by bonded and unbonded CFRP laminates with different pre-stress levels: Experimental and numerical study. Construction and Building Materials, 76, 194–206, 2015. https://doi.org/10.1016/j.conbuildmat.2014.11.070.
- [24] K. A. Harries, A. J. Peck and E. J. Abraham, Enhancing stability of structural steel sections using FRP. Thin-Walled Structures, 47(10), 1092–1101, 2009. https://doi.org/10.1016/j.tws.2008.10.007.
- [25] N. B. Accord and C. J. Earls, Use of fiber-reinforced polymer composite elements to enhance structural steel member ductility. Journal of Composites for Construction, 10(4), 337–344, 2006. https://doi.org/10.1061/(ASCE)10900268(2006)10:4(3 37).
- [26] A. A. E. Damatty, M. Abushagur and M. A. Youssef, Experimental and analytical investigation of steel beams rehabilitated using GFRP sheets. Journal of Materials and Engineering Structures, 3(6), Article 6, 2003
- [27] P. Lacki and A. Derlatka, Influence of PU foam reinforcement of I-beam on buckling resistance. Composite Structures, 202, 201–209, 2018. https://doi.org/10.1016/j.compstruct.2018.01.050.
- [28] P. Lacki, A. Derlatka and J. Winowiecka, Analysis of the composite I-beam reinforced with PU foam with the addition of chopped glass fiber. Composite Structures, 218, 60–70, 2019. https://doi.org/10.10 16/j.compstruct.2019.03.036

- [29] J. Xu, Q. Zhao and P. Qiao, A critical review on buckling and post-buckling analysis of composite structures. Frontiers in Aerospace Engineering, 2(3), 157–168, 2013.
- [30] M. Z. Kabir and A. E. Seif, Lateral-Torsional Buckling of Retrofitted Steel I-Beams Using FRP Sheets. Scientia Iranica, 17(4), 262-272, 2010.
- [31] U. A. Girhammar and D. H. Pan, Exact static analysis of partially composite beams and beam-columns. International Journal of Mechanical Sciences, 49(2), 239-255, 2007. https://doi:10.1016/j.ijmecsci.2006.07.005.
- [32] M. A. Youssef, Analytical prediction of the linear and nonlinear behaviour of steel beams rehabilitated using FRP sheets. Engineering Structures, 28(6), 903-911, 2006. https://doi:10.1016/j.engstruct.2005.10.018.
- [33] K. J. Wong, X. J. Gong, S. Aivazzadeh and M. N. Tamin, Tensile behaviour of anti-symmetric CFRP composite. Procedia Engineering, 10, 1865–1870, 2011. https://doi.org/10.1016/j.proeng.2011.04.310.
- [34] Z. Hashin, Failure criteria for unidirectional fiber composites. Journal of Applied Mechanics, 47(2), 329–334, 1980. https://doi.org/10.1115/1.3153664.
- [35] Dassault Systèmes Simulia Corp., Abaqus 2016 documentation. https://130.149.89.49:2080/v2016/in dex.html, Accessed 13 June 2025.
- [36] J.-O. Majid and M. S. Mohammad Reza, Investigation of defect effects on adhesively bonded joint strength using cohesive zone modeling. Strojnícky časopis –

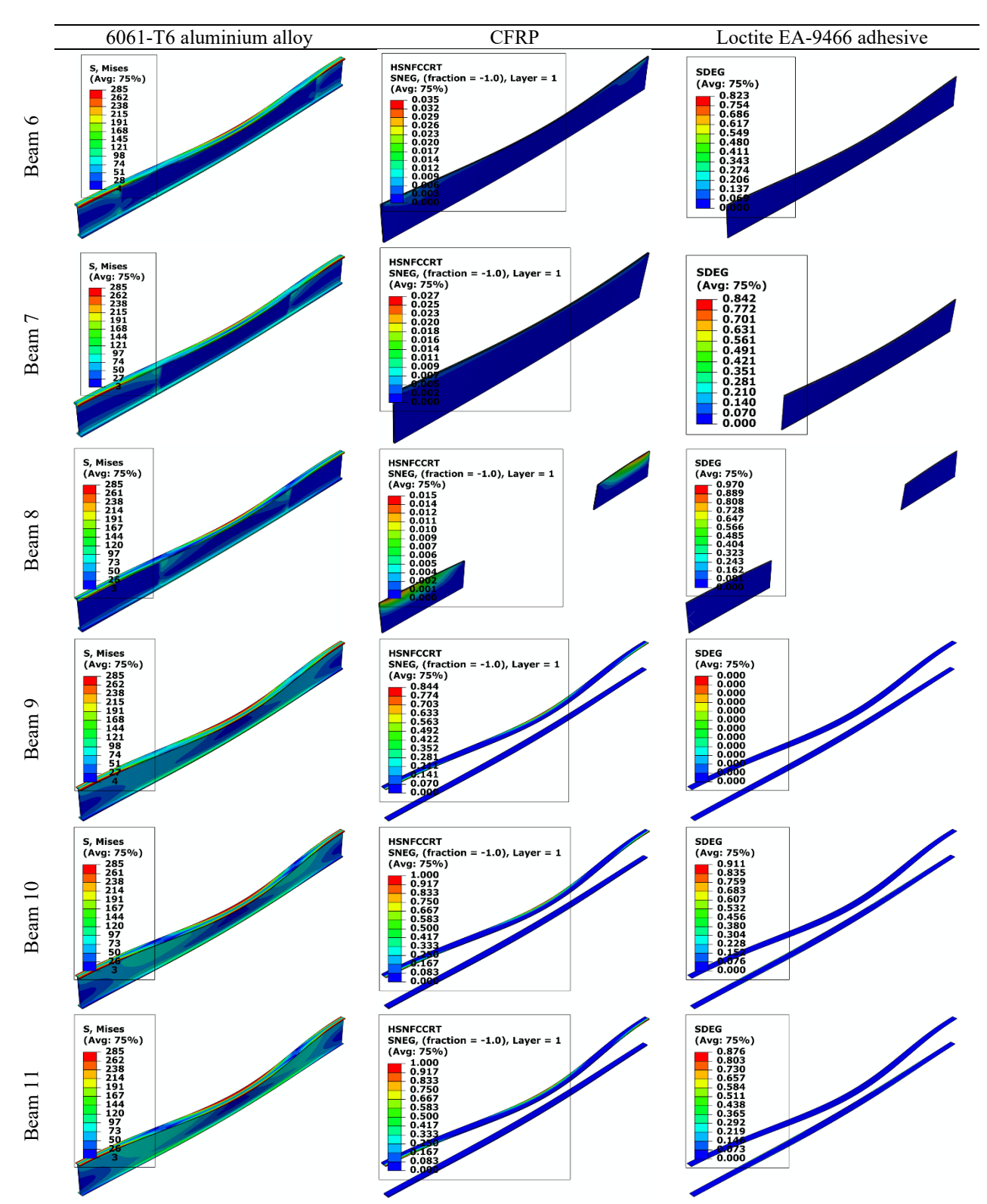
- Journal of Mechanical Engineering, 68(3), 5–24, 2018. https://doi.org/10.2478/scjme-2018-0023.
- [37] H. Taş, Investigation of the defect effects on the load-carrying capacity of butt joints: A numerical study. Hittite Journal of Science and Engineering, 11(3), Article 3, 2024. https://doi.org/10.17350/HJ SE19030000337.
- [38] A. Rahmani and N. Choupani, Experimental and numerical analysis of fracture parameters of adhesively bonded joints at low temperatures. Engineering Fracture Mechanics, 207, 222–236, 2019. https://doi.org/10.1016/j.engfracmech.2018.12.031.
- [39] M. Soltani, A Novel Approach for Lateral Buckling Assessment of Double Tapered Thin-Walled Laminated Composite I-Beams. Mechanics of Advanced Composite Structures, 9(1), 11-23, 2022. https://doi:10.22075/macs.2021.22105.1313.
- [40] A. Lenwari, T. Thepchatri and P. Albrecht, Flexural response of steel beams strengthened with partial-length CFRP plates. Journal of Composites for Construction, 9(4), 296–303, 2005. https://doi.org/10.1061/(ASCE)10900268(2005)9:4(296).
- [41] P. Van Pham, M. Mohareb and A. Fam, Numerical and analytical investigation for ultimate capacity of steel beams strengthened with GFRP plates. Engineering Structures, 243, 112668, 2021. https://doi.org/10.1016/j.engstruct.2021.112668.







Appen A1. Contour plots of Von Mises stress for the aluminium alloy, the fibre compression damage initiation criterion for the CFRP laminate, and the scalar stiffness degradation for the adhesive layer at the onset of LTB



Appen A1. (Cont.) Contour plots of Von Mises stress for the aluminium alloy, the fibre compression damage initiation criterion for the CFRP laminate, and the scalar stiffness degradation for the adhesive layer at the onset of LTB

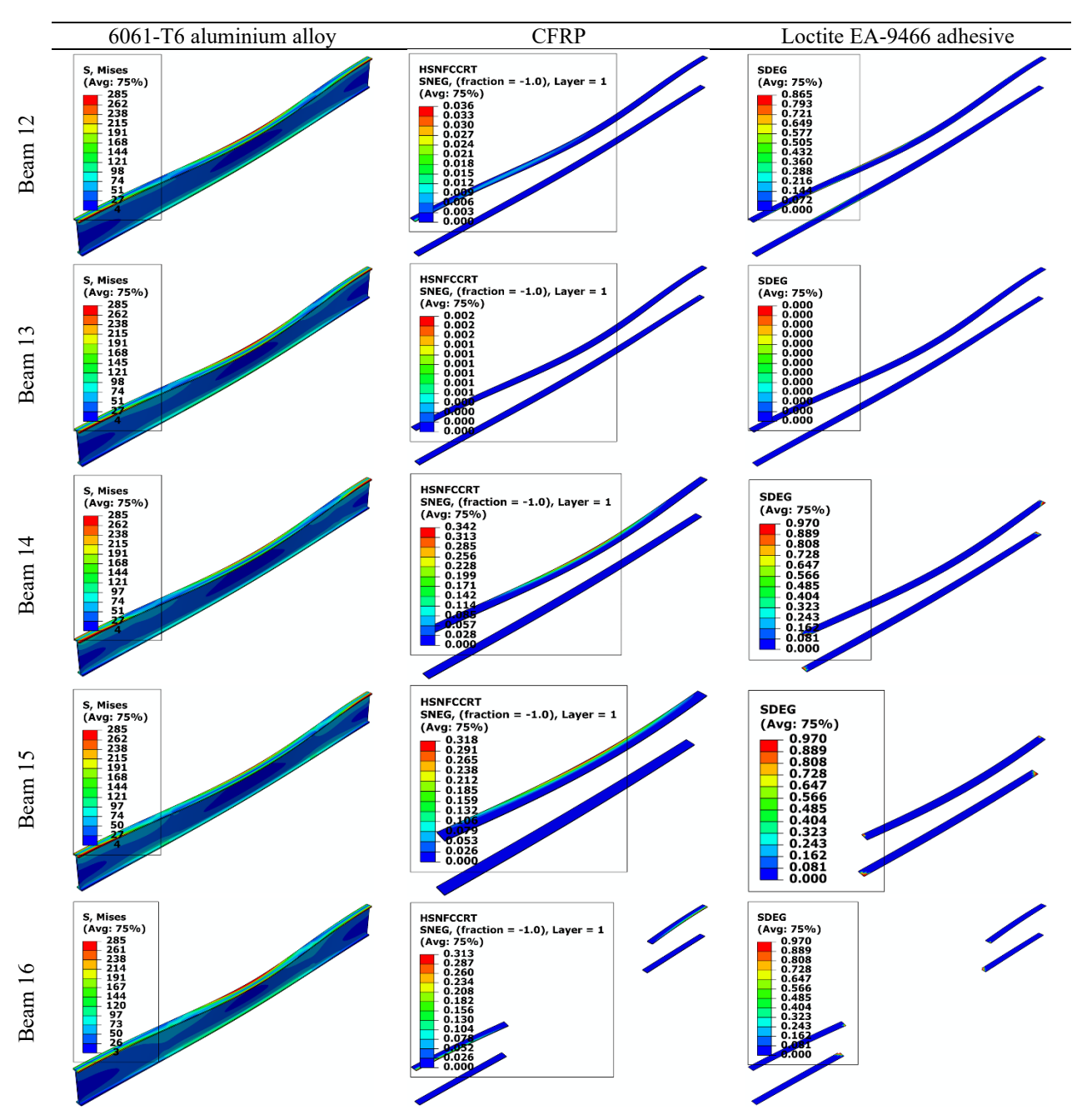


Figure A1. (Cont.) Contour plots of Von Mises stress for the aluminium alloy, the fibre compression damage initiation criterion for the CFRP laminate, and the scalar stiffness degradation for the adhesive layer at the onset of LTB

